Analyst

Accepted Manuscript

ROYAL SOCIETY OF CHEMISTRY

www.rsc.org/analyst

Correlation of Impedance and Effective Electrode Area of Doped PEDOT Modified Electrodes for Brain-Machine Interfaces

Alexander R. Harris[1], Paul J. Molino[2], Robert M.I. Kapsa[2, 3], Graeme M. Clark[4], Antonio G. Paolini[5], Gordon G. Wallace[2]

[1] School of Psychological Science, La Trobe University, Bundoora, Melbourne, Victoria, 3086, Australia

[2] Intelligent Polymer Research Institute, University of Wollongong, Wollongong, NSW, 2522, Australia

[3] Department of Neurosciences, St Vincents Hospital, Melbourne and Department of Medicine University of Melbourne, Fitzroy, Victoria, 3065, Australia

[4] School of Engineering, University of Melbourne, Parkville, Victoria, 3010, Australia

[5] Health Innovations Research Institute, College of Science, Engineering and Health, RMIT University, Bundoora, Victoria, 3083, Australia

Email: alexrharris@gmail.com

Abstract

Electrode impedance is used to assess thermal noise and signal-to-noise ratio for brain-machine interfaces. An intermediate frequency of 1 kHz is typically measured, although other frequencies may be better predictors of device performance. PEDOT-PSS, PEDOT-DBSA and PEDOT-pTs conducting polymer modified electrodes have reduced impedance at 1 kHz compared to bare metal electrodes, but have no correlation with effective electrode area. Analytical solutions to impedance indicate all low-intermediate frequencies can be used to compare electrode area at a series RC circuit, typical of an ideal metal electrode in a conductive solution. More complex equivalent circuits can be used for the modified electrodes, with a simplified Randles circuit applied to PEDOT-PSS and PEDOT-pTs and a Randles circuit including a Warburg impedance element for PEDOT-DBSA at 0 V. The impedance and phase angle at low frequencies using both equivalent circuit models is dependent on electrode area. Low frequencies may therefore provide better predictions of thermal noise and signal-to-noise ratio at modified electrodes. The coefficient of variation of PEDOT-pTs impedance at low frequencies was lower than the other conducting polymers, consistent with linear and steady-state electroactive area measurements. There are poor correlations between impedance and charge density as they are not ideal metal electrodes.

Keywords

Electroactive polymer; Neural prosthesis; Surface analysis; Impedance Spectroscopy; Brain-machine interface

Introduction

Neural implants are being used to record electrical signals in the brain and from peripheral nerves. Neural recordings can be used to control prosthetics, computer interfaces or for understanding neural function. Current clinical devices have low signal-to-noise ratios and performance degrades over time. Improvement of these parameters would result in better user control of their prosthetics, while researchers could gain more reliable data from expensive, and difficult *in vivo* experiments.

Current clinical devices are constructed with platinum electrodes, a highly biocompatible and conductive material. Common research devices include the Utah and Michigan (Neuronexus) style electrode arrays. These electrodes are typically platinum or iridium (allowing conversion to iridium oxide). A large body of work has been aimed at modifying these research electrodes to improve the signal-to-noise ratio, chronic biocompatibility and biostability. In particular, deposition of conducting polymers[1-5], carbon nanotubes[6], graphene[7] and hydrogels[8, 9] has been demonstrated.

The signal measured from a neuron decreases with electrode-neuron distance. Placement of the electrode as close to the target neurons is therefore critical to a good signal-to-noise ratio. However electrode encapsulation with scar tissue excludes the neurons from close electrode proximity, resulting in a decrease in performance over time[10-12]. A recent trend has been inclusion of drug eluting materials incorporating neurotrophic factors to encourage growth of neurons towards the electrode[13, 14]. It is hoped that this will improve the chronic performance of the implant.

Recently we proposed a new method for assessing the acute *in vivo* performance of neural recording devices[15, 16]. By comparing various *in vitro* analytical methods with the electrophysiological response in a rat animal model, important device parameters can be identified for improvement. An analysis of effective electrode area and charge density via optical and electrochemical techniques was then undertaken[17], and we now investigate the impedance characteristics of these devices. The impedance of the electrode is related to the thermal noise and signal-to-noise ratio and it is typically measured at 1 kHz (for instance, most of the electrode modification articles listed above report a decrease in impedance at 1 kHz). However there is little comparison between electrodes to determine the best material or geometry, and a thorough understanding of the relationship between impedance and other electrode parameters is still lacking. In particular, the impedance at other frequencies may be a better predictor of electrophysiological performance. To address this, we measured the impedance spectroscopy over a wide frequency range on the conducting polymer modified electrodes reported previously to compare with the effective electrode area and charge density measurements [17]. PEDOT-PSS was tested as it has been widely used by other research groups, we recommended PEDOT-pTs as a good biostable material[15], and PEDOT-DBSA was also tested as it has a similar structure to pTs.

Results

The impedance of a metal electrode in an electrolyte solution is well known and can be modelled as a series RC circuit [18, 19]. It displays a linear impedance (*Z*) versus frequency (*f*) response, nearly -90° phase angle and linear real (*Z*') versus imaginary (*Z*'') Nyquist impedance (Figure 1a-c). Modification of the electrode with a conducting polymer has been shown to reduce the impedance of the electrode at low and intermediate frequencies [20-22]. We recommended PEDOT-pTs in a previous publication for neural recording applications due to its low impedance, acute biostability during implantation, with low fouling and with a 45 s deposition time, had the smallest error compared to PEDOT-SO_4, polypyrrole (PPy)-pTs and PPy-SO_4 [15]. PEDOT-pTs had a similar impedance at high frequencies compared to uncoated electrodes with a plateau region at intermediate frequencies and rising impedance at low frequencies (Figure 1a). The phase angle approached -90° at low and high frequencies and had a minimum peak at intermediate frequencies (Figure 1b). The Nyquist plot displayed a semi-circle at high to intermediate frequencies and a nearly vertical low frequency response (Figure 1c). The impedance of PEDOT-PSS is very similar to PEDOT-pTs with an impedance plateau region and minimum phase angle peak at intermediate frequencies while the Nyquist plot shows a semi-circle with a vertical response at low frequencies (Figure 1d-f). Increased deposition time (electrode area) decreased the impedance and increased the phase angle at all frequencies tested and the radius of the semi-circle decreased in the Nyquist plot. The impedance of PEDOT-DBSA is again similar, although the plateau region in the impedance versus frequency plot is not as wide and the phase angle minimum peak is also less broad and remains at less negative values at low frequencies (Figure 1g-h). The Nyquist plot of PEDOT-DBSA still possesses a semi-circle at high-intermediate frequencies, however at low frequencies, the response is closer to 45°, more typical of a Warburg impedance (Figure 1i). Increased deposition time of PEDOT-DBSA also produced lower impedance and less negative phase angles at all tested frequencies and reduced the radius of the semi-circle on the Nyquist plot.

Assessment of electrodes for neural recording applications has typically been undertaken by measuring the impedance at 1 kHz to determine the electrode signal-to-noise ratio (SNR) and thermal noise (V_{rms}^{th}),

$$V_{rms}^{th} = \sqrt{k_b T Z \Delta f} \quad (1)$$

where k_b is Boltzmann's constant, T is the absolute temperature and Δf is the measuring bandwidth [23]. All of the modified electrodes presented in Figure 1 have reduced impedance at 1 kHz and moderate differences are present between modified electrodes. We recently measured the effective area of these electrodes by several optical and electrochemical methods[17]. The optical area was seen to increase with deposition time for PEDOT-PSS and PEDOT-DBSA and the linear and steady-state electrochemical area, measured by the reduction of $Ru(NH_3)_6^{3+}$ at fast and slow voltammetric scan

rates respectively, on PEDOT-DBSA modified electrodes also increased with deposition time. Few PEDOT-PSS modified electrodes displayed a steady-state electrochemical response (resulting in fewer data points in Figures 2c, 3c, 5c, 6c and 7c) and the linear electrochemical area had a poor correlation with deposition time and optical area. The impedance at 1 kHz can be plotted against each measured area method (Figure 2 and Table 1). It is clearly seen that the uncoated electrodes have much higher impedance and smaller area than all the modified electrodes, however there is no correlation between impedance at 1 kHz and electrode area measured optically or electrochemically.

The electrode charge density can also be assessed using the different electrode areas[17]. It was shown that all the modified electrodes had larger reduction current charge when measured by cyclic voltammetry, and their charge density was also larger than unmodified electrodes when using the different electrode area measurement methods. Plotting of charge density versus impedance at 1 kHz with PEDOT-pTs, PEDOT-SO_4, PPy-pTs and PPy-SO_4 indicated different materials had different clustering that could be advantageous for neural stimulation and recording from the same electrode [15]. However, these charge density values were calculated from the nominal electrode area. The impedance at 1 kHz versus charge density measured from either optical, steady-state or linear electroactive area is shown in Figure 3. Once again the modified electrodes are clearly separated from the unmodified electrodes with lower impedance and larger charge density when measured by any area method. Yet again, no correlation is seen between impedance at 1 kHz and charge density.

At first glance, the absence of any correlation between impedance and electrode area is confusing, given the well-known relationship between resistance (R_1) and area (A)

$$R_1 = x / \kappa A \tag{2}$$

where x is the material thickness and κ is its conductivity. For an ideal capacitor, impedance is related to its capacitance (C)

$$Z = 1/ j\omega C \tag{3}$$

with ω the perturbation frequency. And the electrode capacitance (C_{dl}) is also related to its area according to,

$$C_{dl} = \varepsilon\varepsilon_0 A / d \tag{4}$$

where ε is the solution dielectric constant, ε_0 is the permittivity of free space and d is the double layer thickness. However, the electrodes used in this and similar studies are more complex. The total impedance is determined from real and imaginary components

$$|Z|^2 = Z'^2 + Z''^2 \tag{5}$$

For a simple RC circuit typical for an uncoated electrode in an electrolyte solution, the total impedance can be determined from

$$|Z| = \sqrt{R_1^2 + \left(\frac{1}{\omega C_{dl}}\right)^2} \quad (6)$$

Although in practice, the capacitance may appear as a constant phase element, modifying the impedance to

$$|Z| = \sqrt{R_1^2 + \left(\frac{1}{\omega^{\alpha} C_{dl}}\right)^2} \quad (7)$$

where α is an exponent equalling 1 for a capacitor and less than one for the non-ideal capacitor. Combining equations 4 and 7 then gives

$$|Z| = \sqrt{R_1^2 + \left(\frac{d}{\omega^{\alpha} \varepsilon \varepsilon_0 A}\right)^2} \quad (8)$$

From this equation, we see that increased frequency reduces the measured impedance as seen in Figure 1a. Increased electrode area can also decrease the electrode impedance, as demonstrated in the surface roughening methods previously described on metal electrodes [24-26]. As the impedance response is linear with frequency, measurement of the impedance at 1 kHz can be used to compare individual electrode areas of ideal metal electrodes in an electrolyte solution. The phase angle (ϕ) at an RC circuit can also be defined

$$\phi = \tan^{-1}\frac{Z''}{Z'} = \tan^{-1}\frac{1}{R_1 \omega C_{dl}} = \tan^{-1}\frac{d}{R_1 \omega \varepsilon \varepsilon_0 A} \quad (9)$$

Indicating low frequencies produce a -90° phase angle, and high frequencies lead to less negative phase angles (Figure 1b). The phase angle will also be sensitive to the electrode area at low frequencies with larger areas creating a less negative phase angle. However, comparison of these ideal metal electrodes in an electrolyte solution at 1 kHz would not display large changes in phase angle.

Modified electrodes have a more complex equivalent circuit, the simplified Randles circuit (Figure 4) can be used for many of these systems, including the PEDOT-pTs and PEDOT-PSS modified electrodes presented here, where

$$Z' = R_s + \frac{R_{ct}}{1 + \omega^2 R_{ct}^2 C_{dl}^2} \quad (10)$$

$$Z'' = -\frac{\omega R_{ct}^2 C_{dl}}{1 + \omega^2 R_{ct}^2 C_{dl}^2} \quad (11)$$

Substituting equation 4 gives

$$Z' = R_s + \frac{R_{ct} d^2}{d^2 + \omega^2 R_{ct}^{\ 2} (\varepsilon\varepsilon_0 A)^2} \tag{12}$$

$$Z'' = -\frac{\omega R_{ct}^{\ 2} (\varepsilon\varepsilon_0 A) d}{d^2 + \omega^2 R_{ct}^{\ 2} (\varepsilon\varepsilon_0 A)^2} \tag{13}$$

With a total impedance

$$|Z|^2 = \left(R_s + \frac{R_{ct} d^2}{d^2 + \omega^2 R_{ct}^{\ 2} (\varepsilon\varepsilon_0 A)^2} \right)^2 + \left(\frac{\omega R_{ct}^{\ 2} (\varepsilon\varepsilon_0 A) d}{d^2 + \omega^2 R_{ct}^{\ 2} (\varepsilon\varepsilon_0 A)^2} \right)^2 \tag{14}$$

As the diffusion layer thickness is relatively small, this can be simplified to

$$\begin{aligned} |Z|^2 &= \left(R_s + \frac{R_{ct}}{\omega^2 R_{ct}^{\ 2} (\varepsilon\varepsilon_0 A)^2} \right)^2 + \left(\frac{\omega R_{ct}^{\ 2} (\varepsilon\varepsilon_0 A)}{\omega^2 R_{ct}^{\ 2} (\varepsilon\varepsilon_0 A)^2} \right)^2 \\ &= \left(R_s + \frac{1}{\omega^2 R_{ct} (\varepsilon\varepsilon_0 A)^2} \right)^2 + \left(\frac{1}{\omega (\varepsilon\varepsilon_0 A)} \right)^2 \end{aligned} \tag{15}$$

This implies that at high frequencies, the total impedance is independent of the electrode area, and little difference will be seen between electrodes. At low frequencies, the electrode area is far more determining of the total impedance. At the intermediate frequency of 1 kHz, there will only be a small effect from electrode area. The large decrease in impedance at 1 kHz typically seen when modifying an electrode is due to the second term appearing in the real impedance (compare equations 8 and 15).

PEDOT-DBSA modified electrodes displayed a Warburg type impedance at low frequencies, this is due to a redox reaction occurring at the testing potential of 0 V. Inspection of the cyclic voltammetry of PEDOT-DBSA modified electrodes displayed a Faradaic process around 0 V [17]. PPy-SO_4 and PPy-pTs also displayed this type of behaviour [15]. This type of system can be modelled by a Randles circuit including a Warburg impedance in series with R_{ct}, the real and imaginary impedances for this circuit are

$$Z' = R_s + \frac{R_{ct} + \sigma\omega^{-1/2}}{(C_{dl}\sigma\omega^{1/2} + 1)^2 + \omega^2 C_{dl}^{\ 2} (R_{ct} + \sigma\omega^{-1/2})^2} \tag{16}$$

$$Z'' = -\frac{\omega C_{dl} (R_{ct} + \sigma\omega^{-1/2})^2 + \sigma\omega^{-1/2} (\omega^{1/2} C_{dl}\sigma + 1)}{(\omega^{1/2} C_{dl}\sigma + 1)^2 + \omega^2 C_{dl}^{\ 2} (R_{ct} + \sigma\omega^{-1/2})^2} \tag{17}$$

Where for a reversible system

$$\sigma = \frac{RT}{n^2 F^2 A\sqrt{2}} \left(\frac{1}{D_O^{1/2} C_O} + \frac{1}{D_R^{1/2} C_R} \right) \tag{18}$$

n being the number of electrons transferred, *R* is the universal gas constant, *F* is Faraday's constant and *D* and *C* are the diffusion coefficient and concentration of the oxidised and reduced species. A similar relationship is seen for quasi-reversible systems[18]. At high frequencies, the total impedance simplifies to

$$|Z|^2 = \left(R_s + \frac{R_{ct}}{1+\omega^2 {R_{ct}}^2 {C_{dl}}^2} \right)^2 + \left(\frac{\omega {R_{ct}}^2 C_{dl}}{1+\omega^2 {R_{ct}}^2 {C_{dl}}^2} \right)^2 \quad (19)$$

where once again the impedance becomes independent of electrode area. At low frequencies,

$$|Z|^2 = \left(R_s + R_{ct} + \sigma\omega^{-1/2} \right)^2 + \left(\sigma\omega^{-1/2} + 2\sigma^2 C_{dl} \right)^2 \quad (20)$$

Substitution of equation 4 produces a similar relationship between the impedance and electrode area as the simplified Randles circuit. To assess the impact of this theory, the impedance of arrays of modified electrodes were tested over a range of frequencies in a simple electrolyte solution. Due to simplicity in data analysis with the current experimental technique, a representative low frequency of 12 Hz was chosen (other values could be used). The impedance at 12 Hz was plotted against the electrode area determined optically and electrochemically (Figure 5 and Table 1). In contrast to the impedance at 1 kHz, there is a clear trend of increased impedance with decreasing electrode area. And fitting of a trendline of the form $Z = \frac{a}{A^2} + \frac{b}{A} + c$ as described in equation 15 gave very good R^2 values (after removal of 1 outlier in Figure 5a, 2 outliers in Figure 5d and 4 outliers in Figure 5e). A trendline of the form $Z = \frac{a}{A}$ gave poorer correlation.

The phase angle of a simplified Randles circuit can also be determined from

$$\phi = \tan^{-1} - \left(\frac{\omega {R_{ct}}^2 (\varepsilon\varepsilon_0 A) d}{d^2 + \omega^2 {R_{ct}}^2 (\varepsilon\varepsilon_0 A)^2} \right) \left(\frac{1}{R_s} + \frac{d^2 + \omega^2 {R_{ct}}^2 (\varepsilon\varepsilon_0 A)^2}{R_{ct} d^2} \right) \quad (21)$$

Simplification by ignoring the small diffusion layer thickness leads to

$$\begin{aligned} \phi &= \tan^{-1} - \left(\frac{\omega {R_{ct}}^2 (\varepsilon\varepsilon_0 A)}{\omega^2 {R_{ct}}^2 (\varepsilon\varepsilon_0 A)^2} \right) \left(\frac{1}{R_s} + \frac{\omega^2 {R_{ct}}^2 (\varepsilon\varepsilon_0 A)^2}{R_{ct}} \right) \\ &= \tan^{-1} - \left(\frac{1}{\omega R_s (\varepsilon\varepsilon_0 A)} + \omega R_{ct} (\varepsilon\varepsilon_0 A) \right) \end{aligned} \quad (22)$$

High frequencies will show no effect of electrode area on phase angle. Intermediate frequencies may show a peak in phase angle dependent on R_{ct}, but again would be of limited use when comparing electrode area. The phase angle at low frequencies will be dependent on electrode area. A similar relationship is seen for a Randles circuit with Warburg impedance. Once again, this theory can be assessed by plots of phase angle at 12 Hz versus electrode area determined optically and electrochemically. Good linear correlations are found in agreement with equation 22 (Figure 6 and

Table 1, removal of 1 outlier in Figure 6a, 1 outlier in Figure 6b and 4 outliers in Figure 6e). The coefficient of variation in impedance and phase angle of each electrode modification is of a similar magnitude and is also comparable to the variation in electrode area determined optically and electrochemically (Table 1 and reference [17]). This implies the measurement of electrode area by each technique is comparable; no additional error sources are being introduced.

The impedance at 12 Hz can also be compared to the charge density measured with different electrode area methods. While the impedance is still lower and the charge density is larger on modified electrodes compared to unmodified electrodes, there is still no correlation between these two properties (Figure 7).

Discussion

The impedance of an electrode is related to its thermal noise and signal-to-noise ratio. Traditionally the impedance of neural implants has been assessed at 1 kHz. However, it is unclear what electrode properties, such as electrode area, are important for improving device performance. Therefore, it is not known what frequencies are the best predictor of electrophysiological performance. Conversely, by not knowing which frequencies are important for controlling the thermal noise (equation 1), the impact of electrode area is also not known. Previous attempts have been made to correct for changes in electrode area after surface modification by using equivalent circuit models from electrical impedance spectroscopy, however this used R_s, which is a poor measurement of electrode area[27]. Ideal metal electrodes in a conductive solution can be modelled as simple RC circuits and the impedance at any low to medium frequency is also a function of electrode area. Measurement of impedance at 1 kHz can then be used to compare different electrodes and so the choice of specific frequency is of less importance. Modifying electrodes such as coating with conducting polymers reduces the impedance at 1 kHz, but also creates a more complex equivalent circuit. Analytically solving the impedance of common Randles equivalent circuits implies the reduction in impedance is due to the presence of the parallel R_{ct} pathway. However, measurement of impedance at this intermediate frequency provides no information on electrode area. In contrast, low frequency measurements (as demonstrated at 12 Hz in this article) displayed very strong correlations between impedance and phase angle versus electrode area determined optically or electrochemically at all modified electrodes. Therefore, if the electrode area is an important factor in determining thermal noise and signal-to-noise ratios, low frequencies would be a better predictor of device performance than intermediate frequencies (ie 1 kHz). Comparison of the electrode impedance at various frequencies to the electrophysiological performance must now be undertaken to give better guidance on electrode design.

The theory detailed here indicates that impedance and phase angle measured at low frequencies provide an electroactive area. The electroactive area is a measurement of the total electrochemically functional electrode area including its roughness, so that regions that are non- or poorly conducting are not included. It was shown previously that reduction of dissolved $Ru(NH_3)_6^{3+}$ can also provide an electroactive area[17]. The area measured in this case includes all regions that can be accessed by the $Ru(NH_3)_6^{3+}$, very small pores will therefore appear non-active. Reduction of $Ru(NH_3)_6^{3+}$ also requires the application of a potential of at least -300 mV vs Ag/AgCl. If the electrode coating is non-homogeneous with regions that are non-conducting or have a slow electron transfer rate, the applied potential is confined to the highly conductive regions, and the electroactive area will only measure these. In contrast, the impedance method used in this article does not include a dissolved redox species, charge is only carried in solution by the movement of the electrolyte. If there are any very small pores in the conducting polymer, their surface area should be measured by impedance. This method also applies an offset potential of 0 V with a 10 mV AC amplitude, and so issues relating to poorly conducting materials is reduced. Nevertheless, the correlation between impedance and linear and steady-state electroactive areas is very strong, implying there are few pores inaccessible to $Ru(NH_3)_6^{3+}$, conducting polymer conductivity and slow electron transfer rate don't have a significant influence in separating these different measurement techniques on these particular modified electrodes.

The conducting polymer modification of neural implants has shown 2 different equivalent circuits; with or without the presence of a Warburg element. The Warburg element is due to a Faradaic reaction occurring at the applied potential of 0 V [17]. This reaction can produce a decrease in impedance, leading to reduced thermal noise and increased signal-to-noise ratio. The charge associated with the reaction can also generate a larger charge density measured by cyclic voltammetry. However, if the Faradaic reaction is not fully reversible, its impact on impedance and charge density will decrease over time. This will lead to degradation in device performance such as increased stimulation threshold and decreased signal-to-noise ratio. In contrast, modification of an electrode through a simplified Randles circuit (no Faradaic reaction present) will also reduce the electrode impedance, but will not be affected by the reversibility of a redox reaction. The performance of this type of electrode (thermal noise and charge density) is then expected to be more stable.

PEDOT-PSS and PEDOT-DBSA both have lower impedance at all low-to-intermediate frequencies than PEDOT-pTs at 45 s deposition times. This indicates they have significantly larger electroactive areas. Their effective electrode areas determined optically and by reduction of $Ru(NH_3)_6^{3+}$ were also larger [17]. This is consistent with the large PSS and DBSA directing growth of the doped conducting polymer out from the electrode surface forming an array of microelectrodes as previously discussed.

Unfortunately their coefficient of variation for each of these measurements was also larger. This increase in coefficient of variation may subsequently lead to a larger error in electrophysiological performance. And so once again we recommend a 45 s deposition of PEDOT-pTs as the best electrode modification method from those tested to date.

No correlations were seen between impedance at any frequency and charge density. We previously reported no correlation between effective electrode area and charge density either [17]. As previously discussed, if the charge density were solely due to electrode capacitance, it would be related to the electrode area and therefore the impedance at low frequency [17]. However, none of the electrodes presented here are ideal RC circuits, they include other charge transfer reactions such as the reduction of oxygen or the conducting polymer. The charge determined by cyclic voltammetry is therefore not highly correlated with electrode area as measured optically or electrochemically.

Conclusion

Neural implants are used to record the electrical signal of neurons in the central and peripheral nervous system. The impedance of the electrode is usually measured as it is related to the thermal noise and signal-to-noise ratio. Conducting polymer modified electrodes have reduced impedance at 1 kHz compared to bare metal electrodes. Analytical solutions of electrode impedance at a series RC circuit, typical of an ideal metal electrode in a conductive solution, indicate impedance at all low-intermediate frequencies can be used to compare electrode area. Modification of the electrode can be modelled by more complex equivalent circuits. A simplified Randles circuit can be used to model PEDOT-PSS and PEDOT-pTs at 0 V while a Randles circuit including a Warburg impedance element can be used for PEDOT-DBSA. The impedance at 1 kHz on these electrodes is reduced in comparison to unmodified electrodes, but there is little difference between modified electrodes. In contrast, impedance and phase angle at low frequencies with both equivalent circuit models is dependent on electrode area. Therefore, the impedance and phase angle at low frequencies may be a better predictor of electrophysiological performance. The coefficient of variation of PEDOT-pTs impedance at low frequencies was lower than the other conducting polymers, consistent with linear and steady-state electroactive area measurements. Charge density measurements show poor correlations with impedance as they are not ideal metal electrodes.

Experimental Section

3,4-ethylenedioxythiophene (EDOT), poly(styrenesulfonate) (PSS, MW = 70,000), sodium dodecylbenzenesulfonate (NaDBSA), sodium *para*-toluene sulfonate (Na_2pTS) (Sigma-Aldrich) and 99.0 % di-sodium phosphate (Fluka) were used as received. Electrodes were coated as described previously[17], briefly polymer coatings were deposited on 32, 413 μm^2 nominal geometric area platinum electrodes (Neuronexus Technologies – A4x8-5mm-200-200-413). Potentiostatic growth

via a potentiostat (CH660D, CH Instruments) was performed in a three-electrode configuration using one microelectrode as the working electrode, Ag/AgCl (3 M NaCl) as reference electrode and Pt mesh as counter electrode. Solutions were degassed for 30 minutes with nitrogen before depositing the electrode coatings. All polymers were deposited at 1 V vs Ag/AgCl. PEDOT-PSS and PEDOT-DBSA were deposited for 4 different times (15, 30, 45 or 60 s), PEDOT-pTs was deposited for 45s as recommended in our previous article [15]. 2 probes were coated with PEDOT-PSS and 2 with PEDOT-DBSA, 4 electrode sites coated at each deposition time in a staggered array as previously described[15], leaving 12 uncoated platinum electrodes and 4 PEDOT-pTS coated electrodes as controls.

Electrodes areas and charge densities were determined optically and electrochemically as described previously [17]. Images were obtained on a BX61 optical microscope (Olympus) and the area measured with ImageJ. The resolution and error in the optical area measurement is controlled by the microscopes numerical aperture; with a resolution of less than 0.5 μm, it will have negligible influence on the recorded values. Electrochemical area was determined by the reduction of 5 mM $Ru(NH_3)_6^{3+}$ in non-degassed, 0.3 M phosphate buffer. A CHI660B potentiostat with CHI684 multiplexer (CH Instruments) were used to perform cyclic voltammetry and electrochemical impedance spectroscopy (EIS) at each of the individually addressable working electrode sites [15, 16]. A 3 electrode configuration was used with a Ag/AgCl (3 M KCl) reference and Pt mesh counter electrode. Charge density measurements were performed using cyclic voltammetry over a range of 0.8 to -0.8 V vs Ag/AgCl at a scan rate of 100 mV s^{-1}. Electroactive area measurements were undertaken over a range of 0 to -0.5 V varying the scan rate from 10 mV s^{-1} to 1 V s^{-1}. The voltammetric peak height at fast scan rates was used to calculate the linear area while measurement of the steady-state current at slow scan rates was used to calculate the steady-state area. A more detailed discussion of the electroactive area measurements can be found in [17]. EIS was undertaken at 0 V with a 10 mV amplitude over a frequency range of 10-100,000 Hz.

Acknowledgements

The authors acknowledge the support of the Australian Research Council through the Centre of Excellence for Electromaterials Science.

References

1. K. A. Ludwig, J. D. Uram, J. Yang, D. C. Martin and D. R. Kipke, *Journal of Neural Engineering*, 2006, **3**, 59.
2. R. A. Green, N. H. Lovell, G. G. Wallace and L. A. Poole-Warren, *Biomaterials*, 2008, **29**, 3393-3399.
3. Y. P. Kayinamura, M. Ovadia, D. Zavitz and J. F. Rubinson, *ACS Applied Materials & Interfaces*, 2010, **2**, 2653-2662.

4. P. A. Forcelli, C. T. Sweeney, A. D. Kammerich, B. C. W. Lee, L. H. Rubinson, Y. P. Kayinamura, K. Gale and J. F. Rubinson, *Journal of Biomedical Materials Research Part A*, 2012, **100A**, 3455-3462.
5. H. S. Mandal, G. L. Knaack, H. Charkhkar, D. G. McHail, J. S. Kastee, T. C. Dumas, N. Peixoto, J. F. Rubinson and J. J. Pancrazio, *Acta Biomaterialia*, 2014, **10**, 2446–2454.
6. G. Gabriel, R. Gómez, M. Bongard, N. Benito, E. Fernández and R. Villa, *Biosensors and Bioelectronics*, 2009, **24**, 1942-1948.
7. L. H. Hess, M. Jansen, V. Maybeck, M. V. Hauf, M. Seifert, M. Stutzmann, I. D. Sharp, A. Offenhäusser and J. A. Garrido, *Advanced Materials*, 2011, **23**, 5045-5049.
8. R. A. Green, S. Baek, L. A. Poole-Warren and P. J. Martens, *Science and Technology of Advanced Materials*, 2010, **11**, 014107.
9. D.-H. Kim, M. Abidian and D. C. Martin, *Journal of Biomedical Materials Research Part A*, 2004, **71A**, 577-585.
10. W. Grill and J. Thomas Mortimer, *Annals of Biomedical Engineering*, 1994, **22**, 23-33.
11. P. J. Rousche and R. A. Normann, *Journal of Neuroscience Methods*, 1998, **82**, 1-15.
12. S. Suner, M. R. Fellows, C. Vargas-Irwin, G. K. Nakata and J. P. Donoghue, *Neural Systems and Rehabilitation Engineering, IEEE Transactions on*, 2005, **13**, 524-541.
13. R. T. Richardson, B. Thompson, S. Moulton, C. Newbold, M. G. Lum, A. Cameron, G. Wallace, R. Kapsa, G. Clark and S. O'Leary, *Biomaterials*, 2007, **28**, 513-523.
14. B. C. Thompson, S. E. Moulton, R. T. Richardson and G. G. Wallace, *Biomaterials*, 2011, **32**, 3822-3831.
15. A. R. Harris, S. J. Morgan, J. Chen, R. M. I. Kapsa, G. G. Wallace and A. G. Paolini, *Journal of Neural Engineering*, 2013, **10**, 016004.
16. A. R. Harris, S. J. Morgan, G. G. Wallace and A. G. Paolini, *Journal of Visualized Experiments*, 2014, e51084.
17. A. R. Harris, P. J. Molino, R. M. I. Kapsa, G. M. Clark, A. G. Paolini and G. G. Wallace, *Analytical Chemistry*, 2015, **87**, 738-746.
18. A. J. Bard and L. R. Faulkner, *Electrochemical Methods*, Wiley, New York, 2001.
19. E. T. McAdams, A. Lackermeier, J. A. McLaughlin, D. Macken and J. Jossinet, *Biosensors and Bioelectronics*, 1995, **10**, 67-74.
20. X. Cui, V. A. Lee, Y. Raphael, J. A. Wiler, J. F. Hetke, D. J. Anderson and D. C. Martin, *Journal of Biomedical Materials Research*, 2001, **56**, 261-272.
21. X. Cui, J. F. Hetke, J. A. Wiler, D. J. Anderson and D. C. Martin, *Sensors and Actuators A: Physical*, 2001, **93**, 8-18.
22. X. Cui and D. C. Martin, *Sensors and Actuators B: Chemical*, 2003, **89**, 92-102.
23. G. Baranauskas, E. Maggiolini, E. Castagnola, A. Ansaldo, A. Mazzoni, G. N. Angotzi, A. Vato, D. Ricci, S. Panzeri and L. Fadiga, *Journal of Neural Engineering*, 2011, **8**, 066013.
24. D. A. Robinson, *Proceedings of the IEEE*, 1968, **56**, 1065-1071.
25. V. Pollak, *Medical and Biological Engineering*, 1974, **12**, 460-464.
26. V. Pollak, *Medical and Biological Engineering and Computing*, 1974, **12**, 606-612.
27. Y. Lu, T. Li, X. Zhao, M. Li, Y. Cao, H. Yang and Y. Y. Duan, *Biomaterials*, 2010, **31**, 5169–5181.

Figure Captions

Figure 1: Typical impedance response of electrodes in 0.3 M Na_2HPO_4 at 0 V and 10 mV amplitude (a-c) uncoated and PEDOT-pTs deposited for 45 s, (d-f) PEDOT-PSS and (g-i) PEDOT-DBSA at varying deposition times.

Figure 2: Comparison of impedance at 1 kHz measured in 0.3 M Na_2HPO_4 at 0 V and 10 mV amplitude with electrode area measured (a-b) optically or by electrochemical reduction of 5 mM $Ru(NH_3)_6^{3+}$ at (c-d) steady state or (e-f) linear diffusion. (a, c and e) PEDOT-PSS and (b, d and f) PEDOT-DBSA modified electrodes.

Figure 3: Comparison of impedance at 1 kHz measured in 0.3 M Na_2HPO_4 at 0 V and 10 mV amplitude versus charge density with an electrode area measured (a-b) optically or by electrochemical reduction of 5 mM $Ru(NH_3)_6^{3+}$ at (c-d) steady state or (e-f) linear diffusion. (a, c and e) PEDOT-PSS and (b, d and f) PEDOT-DBSA modified electrodes.

Figure 4: Simplified Randles Circuit.

Figure 5: Comparison of impedance at 12 Hz measured in 0.3 M Na_2HPO_4 at 0 V and 10 mV amplitude with electrode area measured (a-b) optically or by electrochemical reduction of 5 mM $Ru(NH_3)_6^{3+}$ at (c-d) steady state or (e-f) linear diffusion. (a, c and e) PEDOT-PSS and (b, d and f) PEDOT-DBSA modified electrodes. The fitted trendline is of the form $Z = \frac{a}{A^2} + \frac{b}{A} + c$.

Figure 6: Comparison of phase angle at 12 Hz measured in 0.3 M Na_2HPO_4 at 0 V and 10 mV amplitude with electrode area measured (a-b) optically or by electrochemical reduction of 5 mM $Ru(NH_3)_6^{3+}$ at (c-d) steady state or (e-f) linear diffusion. (a, c and e) PEDOT-PSS and (b, d and f) PEDOT-DBSA modified electrodes. The fitted trendline is linear.

Figure 7: Comparison of impedance at 12 Hz measured in 0.3 M Na_2HPO_4 at 0 V and 10 mV amplitude versus charge density with an electrode area measured (a-b) optically or by electrochemical reduction of 5 mM $Ru(NH_3)_6^{3+}$ at (c-d) steady state or (e-f) linear diffusion. (a, c and e) PEDOT-PSS and (b, d and f) PEDOT-DBSA modified electrodes.

Figures

Table 1. Average, standard deviation and coefficient of variation of impedance (kOhm).

Polymer coating	Impedance 1kHz			Impedance 12 Hz			Phase Angle 12 Hz		
	Ave	SD	CV	Ave	SD	CV	Ave	SD	CV
15s PEDOT-PSS	26.3	2.3	0.09	145.07	36.72	0.25	-75.9	4.4	0.06
30s PEDOT-PSS	24.0	3.9	0.16	57.77	8.11	0.14	-59.5	8.4	0.14
45s PEDOT-PSS	32.9	21.9	0.67	55.84	22.06	0.40	-42.9	13.6	0.32
60s PEDOT-PSS	25.6	7.7	0.30	36.97	6.00	0.16	-32.4	7.7	0.24
45s PEDOT-pTs	40.9	11.7	0.29	336.35	18.15	0.05	-78.0	3.7	0.05
Uncoated	309.4	14.7	0.05	23599.94	6585.29	0.28	-71.7	22.5	0.31
15s PEDOT-DBSA	57.8	16.4	0.28	469.71	64.80	0.14	-49.3	9.7	0.20
30s PEDOT-DBSA	51.9	16.4	0.32	298.95	43.90	0.15	-39.6	10.9	0.28
45s PEDOT-DBSA	39.3	7.1	0.18	202.08	38.67	0.19	-38.1	4.5	0.12
60s PEDOT-DBSA	40.8	10.5	0.26	168.67	48.27	0.29	-33.7	2.0	0.06
45s PEDOT-pTs	70.8	5.6	0.08	816.24	57.71	0.07	-53.0	1.4	0.03
Uncoated	299.3	18.9	0.06	23918.80	6894.05	0.29	-81.4	16.1	0.20

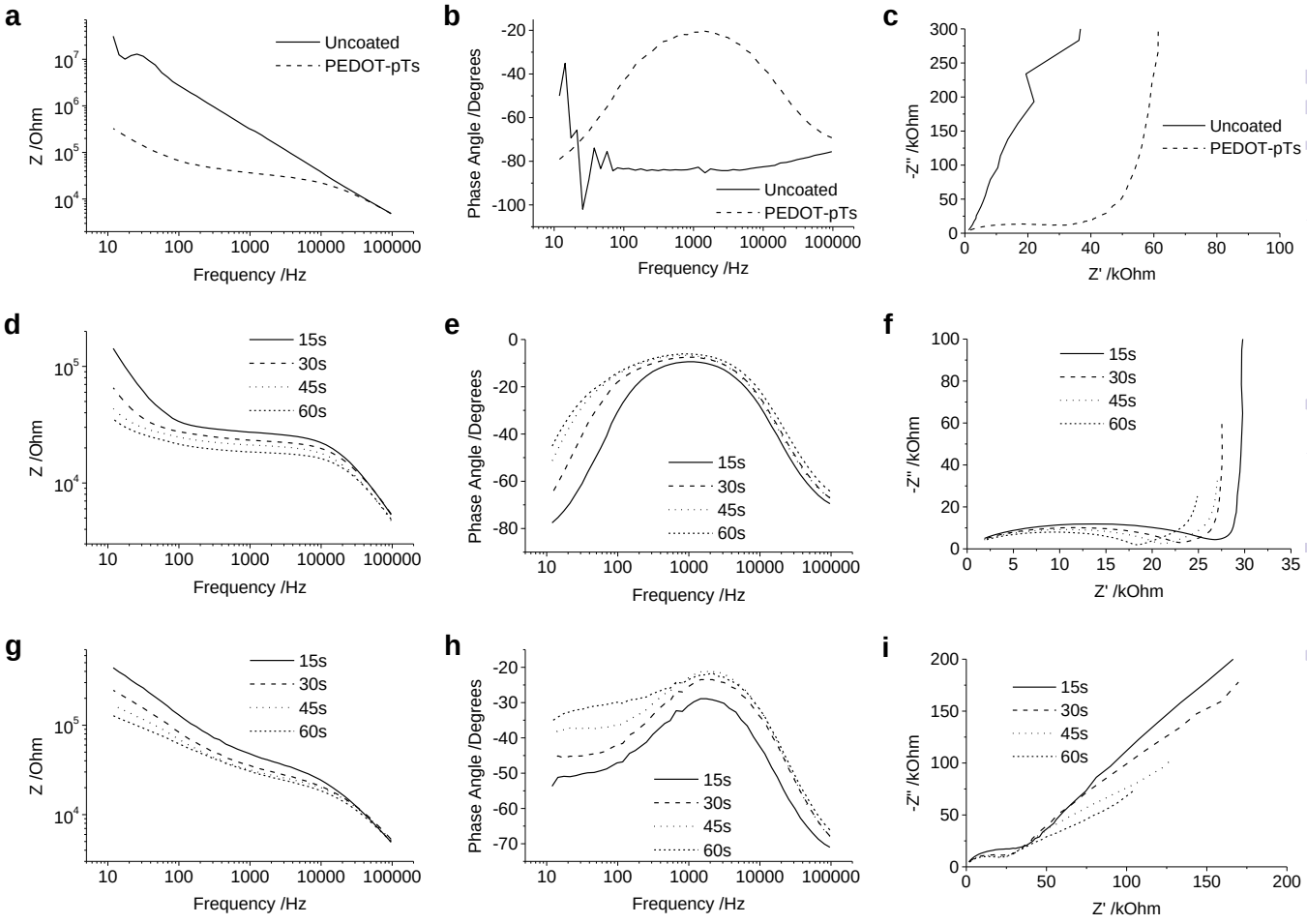

Figure 1

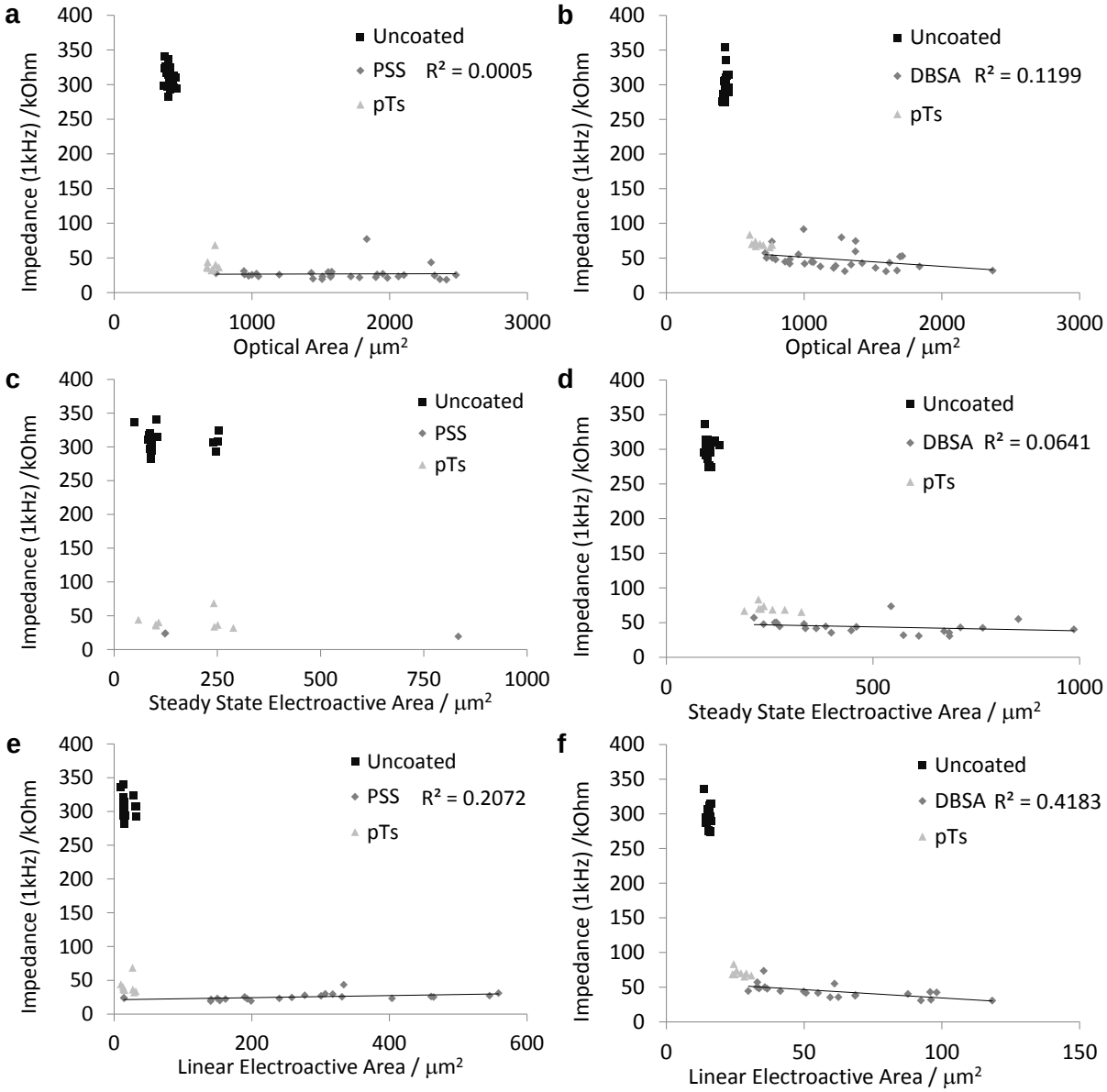

Figure 2

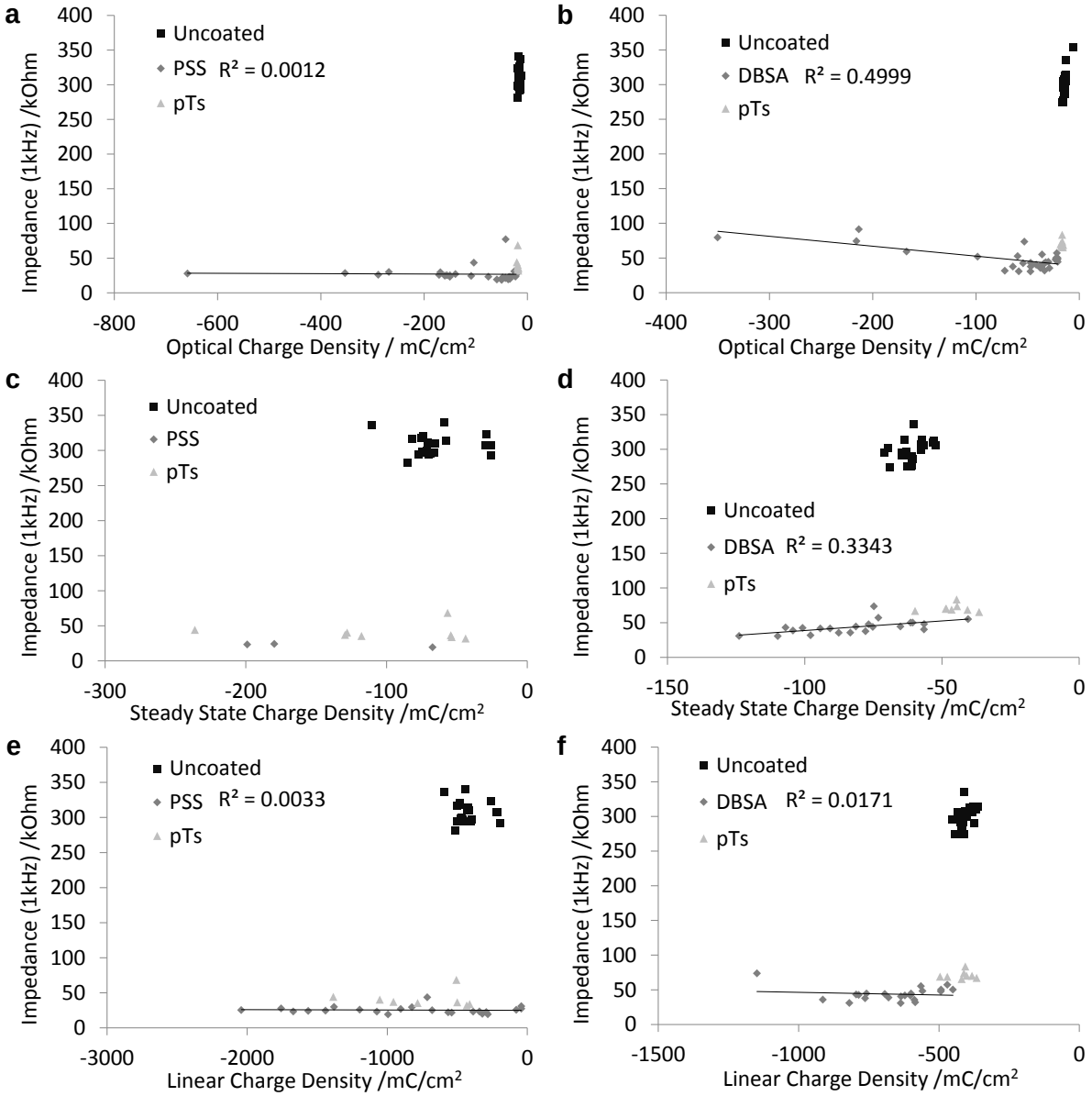

Figure 3

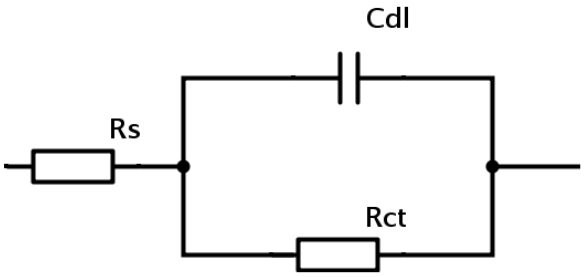

Figure 4

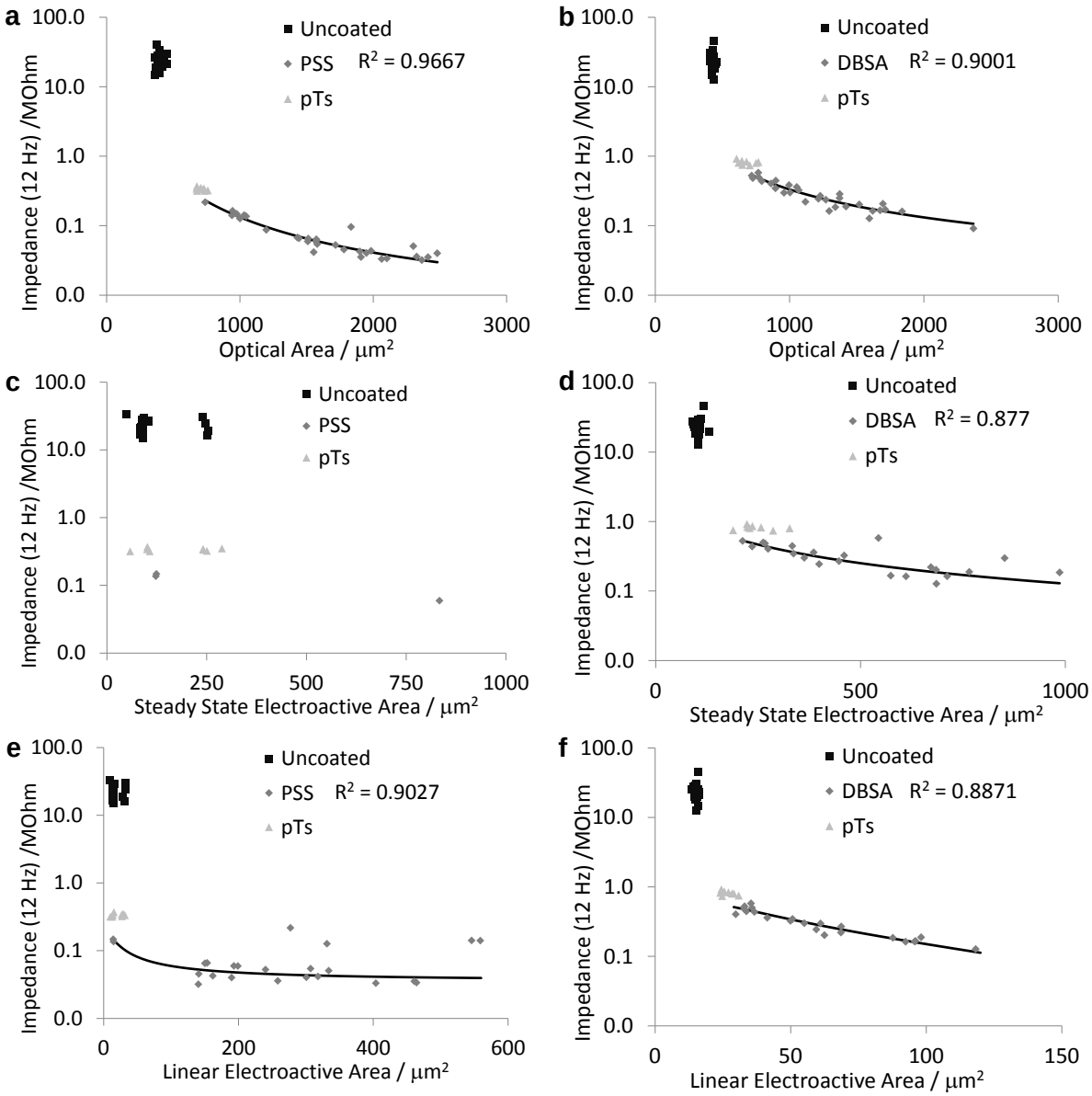

Figure 5

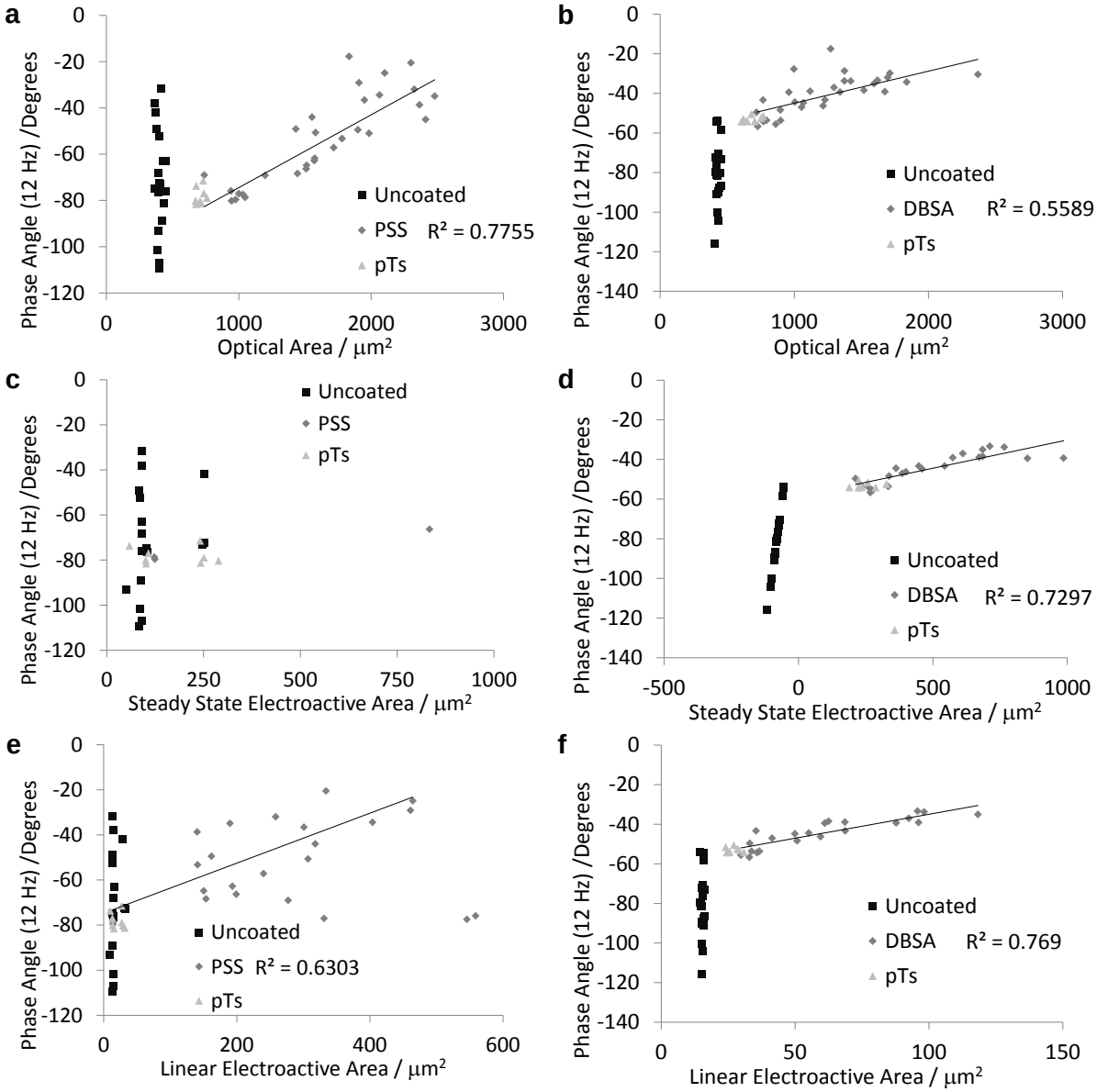

Figure 6

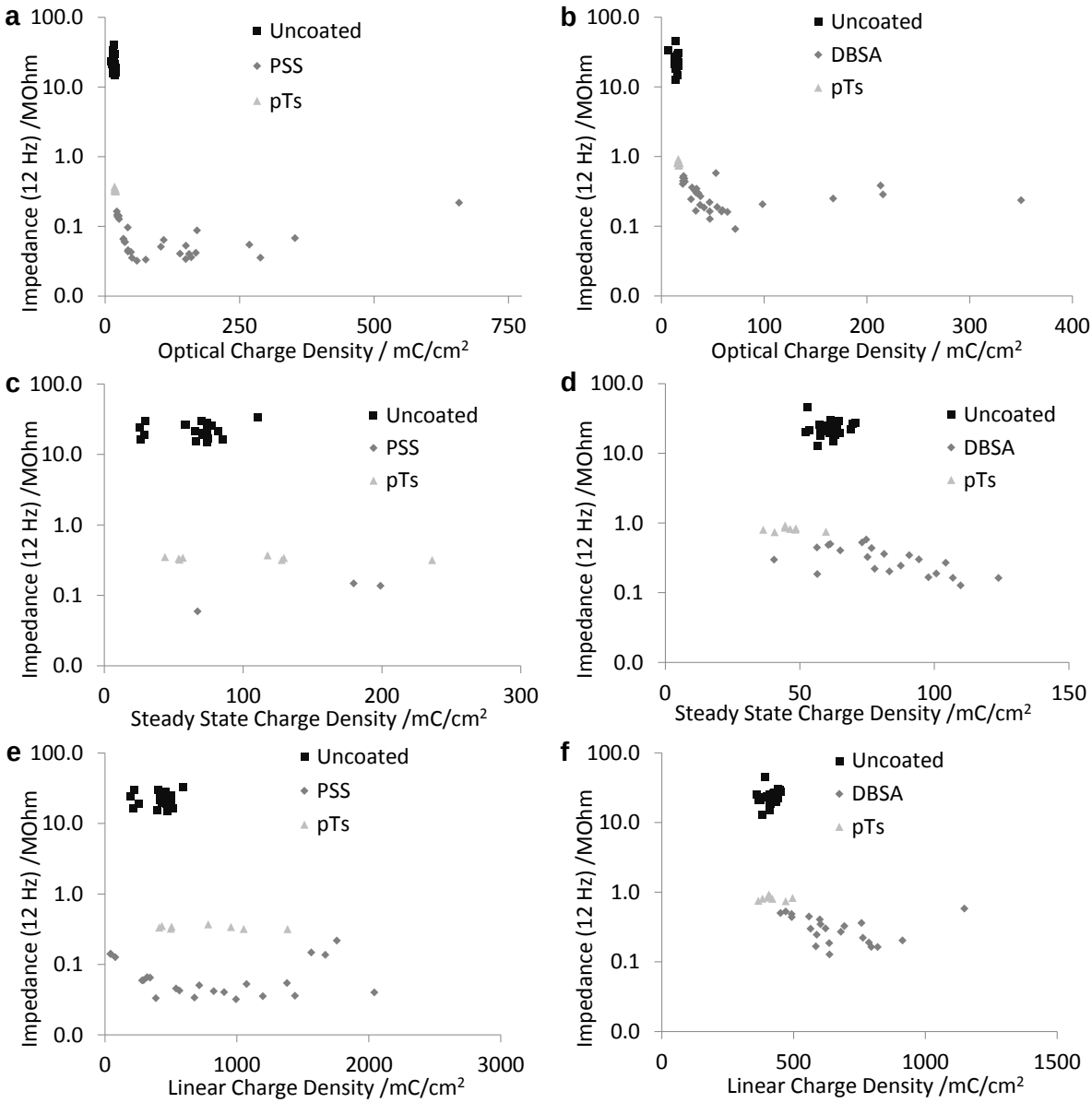

Figure 7

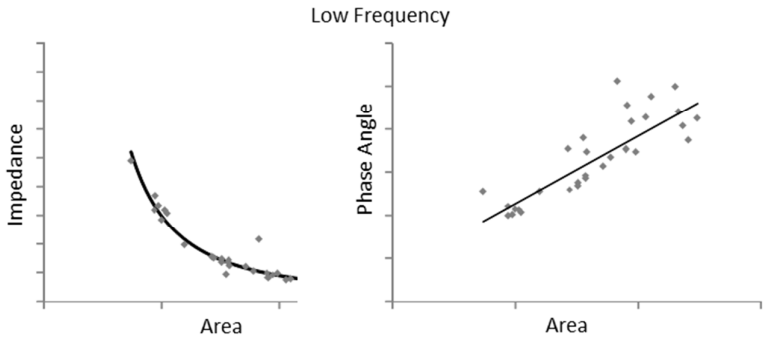

An analytical solution to impedance allows correlation of effective electrode area with impedance and phase angle at low frequencies